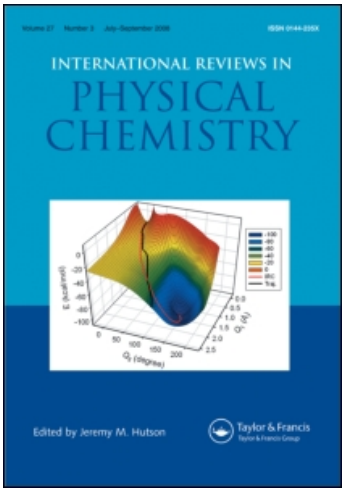

International Reviews in Physical Chemistry
Publication details, including instructions for authors and subscription information:
http://www.informaworld.com/smpp/title~content=t713724383

Excitation functions of elementary chemical reactions: A direct link from crossed-beam dynamics to thermal kinetics ?

Kopin Liu[a]
[a] Institute of Atomic and Molecular Sciences, Academia Sinica, Taipei, Taiwan

Online publication date: 26 November 2010

To cite this Article Liu, Kopin(2001) 'Excitation functions of elementary chemical reactions: A direct link from crossed-beam dynamics to thermal kinetics ?', International Reviews in Physical Chemistry, 20: 2, 189 — 217
To link to this Article: DOI: 10.1080/01442350110034057
URL: http://dx.doi.org/10.1080/01442350110034057

INT. REVIEWS IN PHYSICAL CHEMISTRY, 2001, VOL. 20, NO. 2. 189–217

Excitation functions of elementary chemical reactions: a direct link from crossed-beam dynamics to thermal kinetics?

KOPIN LIU

Institute of Atomic and Molecular Sciences, Academia Sinica, Taipei 106, Taiwan

The excitation function refers to the translational energy dependence of the integral cross-section of a biomolecular collision process. Exemplified by a number of elementary chemical reactions, the information content of excitation functions is critically surveyed. Particular emphasis is placed on the close comparison with the available thermal kinetics data. The reactivity for an activated reaction was found to depend sensitively on the rotational state of the reagent, indicative of stereodynamical effects. The intramolecular isotope branching ratio, for the reaction A+HD, exhibits a strong dependence on the collision energy. Its isotopic propensity reverses between a non-rotating and a rotating reagent. By way of contrast, the reactive behaviour of a barrierless reaction shows little dependence on the initial rotational state, and the intramolecular isotope branching ratio instead becomes nearly independent of the collision energy. In this case, the excitation function obtained from crossed-beam experiments then provides a direct and reliable route to compare with available thermal rate constants or to extrapolate kinetics to a wider temperature range.

Contents

1. Introduction: route from dynamics to kinetics

Gas-phase reaction dynamics is the modern-day approach towards the chemical kinetics problem (Levine and Bernstein 1987). Its fundamental aim is to gain an

International Reviews in Physical Chemistry ISSN 0144-235X print/ISSN 1366-591X online © 2001 Taylor & Francis Ltd
http://www.tandf.co.uk/journals
DOI: 10.1080/01442350110034057

understanding of the mechanism that governs the chemical reactivity of elementary processes. To this end, it is necessary experimentally to control the internal state of reagents with a well-defined initial collision energy, and to probe the reaction product in a state-specific manner under the so-called 'single-collision' conditions, in which the process of interest is isolated and all other secondary processes are eliminated. These ideal experimental conditions are best met by the crossed-molecular-beam technique. On the other hand, the wide range of applications of chemical kinetics to real-world problems, such as those in combustion, atmospheric chemistry, astrophysical chemistry and chemical vapour deposition processes, are mostly concerned just about the thermal kinetic behaviour. The physical quantity of interest is how chemical reaction rates vary with ambient temperature and pressure conditions. In interpreting or modelling those natural or man-made phenomena, it is a general practice to assume that the translational energy and the internal state distributions of reagents are in thermal equilibrium at the ambient temperature. Nevertheless, the validity of this assumption may not hold in some cases, calling for more detailed dynamics information. For example, owing to the low-density environment in space, the application to the astrochemical problem may sometimes need to go beyond the thermal rate constant by considering state-specific rate coefficients.

The connection between dynamics and kinetics is through the well-known Boltzmann averaging of the individual state-to-state rate coefficients k_{if} over the thermal population of the reagents' states (Levine and Bernstein 1987):

$$k(T) = \sum_i P_i(T) \sum_f k_{if}(T), \tag{1}$$

where $k(T)$ is the thermal rate constant at temperature T, $k_{if}(T)$ is the corresponding state-to-state rate coefficient from the initial reagent state i to the final product state f, and $P_i(T)$ denotes the normalized Boltzmann factor of the internal state i of the reagent. A physical quantity obtainable from a crossed-beam scattering experiment is the excitation function, that is the dependence of the reaction cross-section on the initial translational energy E_c (Gonzalez-Urena 1987, 1992). This quantity is related to the state-to-state rate coefficient by

$$k_{if}(T) = \frac{\langle v \rangle}{(kT)^2} \int_0^\infty \sigma_{if}(E_c) E_c \exp\left(-\frac{E_c}{kT}\right) \mathrm{d}E_c, \tag{2}$$

where $\langle v \rangle = (8\,kT/\pi\mu)^{1/2}$ is the average relative velocity of reagents at the temperature T, and k is the Boltzmann constant. Since the Boltzmann averaging over the internal state and the initial translational (or collision) energy distributions in equations (1) and (2) respectively are for the reagents only, it is convenient to consider just the reagent state-specific rate coefficients by summing all product states, namely

$$k(T) = \sum_i P_i(T) k_i(T) \tag{3}$$

and

$$k_i(T) = \frac{\langle v \rangle}{(kT)^2} \int_\sigma^\infty \sigma_i(E_c) E_c \exp\left(-\frac{E_c}{kT}\right) \mathrm{d}E_c. \tag{4}$$

Equation (1) and (2) (or equations (3) and (4)) thus furnish the route from state-to-state cross-sections (or state-specific cross-sections) to the thermal kinetic rate.

Although the above connection from dynamics to kinetics has long been established, it is seldom used in practice by experimentalists to check the consistency of the two sets of data (dynamics versus kinetics) or to gain further insights. One of the main reasons might be the lack of a complete set of state-specific cross-sections. Experimentally, the reaction excitation function is often obtained from a crossed-beam experiment. The use of supersonic molecular beams for better control of collision energy resolution also dictates most of the reagents residing in the ground state. The corresponding state-specific cross-section is denoted as $\sigma_0(E_c)$. One can then re-express equation (3) as

$$k(T) = k_0(T) \sum_i \frac{P_i(T) k_i(T)}{k_0(T)}, \tag{5}$$

where $k_0(T)$ corresponds to the ground state-specific rate coefficient at temperature T. Since the sum of the normalized Boltzmann factors is unity for all temperatures, that is $\Sigma_i P_i(T) = 1$, the comparison of the beam-derived rate coefficient $k_0(T)$ with the thermal kinetics data $k(T)$ can then lead to invaluable information. For example, if $k(T) \approx k_0(T)$, then, from equation (5), one can conclude that $k_i(T)/k_0(T) \approx$ constant for all i, or the reactivities of different reagent states are not very different. On the other hand, if $k_0(T)$ exhibits a different temperature dependence from $k(T)$, then the state-specific rate coefficients must depend sensitively on the initial reagent states. This is the strategy that we have taken and applied to a number of elementary chemical reactions over the past few years. This review summarizes the main findings and illustrates what kinds of new insights could be gained through such an approach. We shall also examine the condition under which the dynamical information obtained from a crossed-beam experiment can be used reliably to compare with or to extrapolate to the available thermal kinetics data, that is the question mark in the title of this review. Although the examples shown below are mostly taken from this laboratory, it should be emphasized that several other groups (Naulin and Costes 1999, Geppert *et al.* 2000, Vetter *et al.* 2000) recently also adopted this approach. Some of these very exciting results will be highlighted here.

Before considering specific examples, it is instructive to examine a few special cases for deeper appreciation of the relationship between the excitation function and thermal rate constant. For simplicity let us assume that $k_i(T) = k_0(T)$; then

$$k(T) = \frac{1}{\sqrt{\pi\mu}} \left(\frac{2}{kT}\right)^{3/2} \int_0^\infty \sigma_0(E_c) E_c \exp\left(-\frac{E_c}{kT}\right) dE_c. \tag{6}$$

Table 1 lists some analytical results of the predicted temperature dependences of thermal rate constants for a few model excitation functions. Model (1) is the venerable line-of-centre reaction mechanism (Levine and Bernstein 1987) which assumes that reaction occurs whenever the projection of the relative collision energy along the line of centres of the two reagents exceeds the activation barrier. Models (2) and (3) represent two variants, which account for steric effects. What differentiates them lies in the anisotropy of the potential energy surface (PES) in the transition-state region, that is the bending potential at the reaction saddle point for a three-atom reaction system or the orientation dependence of the activation barrier to reaction. As shown in table 1, the connection between the activation energy E_a in kinetics and the reaction barrier ε_0 in dynamics depends on the bending potential at the saddle point. According to these models, the non-Arrhenius behaviour of

Table 1. Summary of the bending potential $V(\gamma)$, excitation function $\sigma(E_c)$, thermal rate constant $k(T)$ and activation energy $E_a = -k[\mathrm{d}(\ln k(T))/\mathrm{d}(1/T)]$ for a few activated reaction models. $\sigma_{HS} = \pi d^2$ and $\langle v \rangle = (8kT/\pi\mu)^{1/2}$.

Model	$V(\gamma)$	$\sigma(E_c)$	$k(T)$	E_a
1	ε_0	$\sigma_{HS}(E_c-\varepsilon_0)/E_c$	$\sigma_{HS}\langle v\rangle \exp(-\varepsilon_0/kT)$	$\varepsilon_0+kT/2$
2	$\varepsilon_0+\varepsilon_0'(1-\cos\gamma)$	$(\sigma_{HS}/2\varepsilon_0')(E_c-\varepsilon_0)^2/E_c$	$\sigma_{HS}(kT/\varepsilon_0')\langle v\rangle \exp(-\varepsilon_0/kT)$	$\varepsilon_0+3kT/2$
3	$\varepsilon_0+\varepsilon_0'(1-\cos\gamma)^2$	$[2\sigma_{HS}/3(\varepsilon_0')^{1/2}](E_c-\varepsilon_0)^{3/2}/E_c$	$(\sigma_{HS}/2)(\pi kT/\varepsilon_0')^{1/2}\langle v\rangle \exp(-\varepsilon_0/kT)$	ε_0+kT

thermal rate constants, that is that the activation energy E_a varies for different temperature ranges, should be a norm, instead of an exception, for an activated reaction.

Not shown in the table are the models for a chemical reaction governed by the long-range attractive potential. The cross-section of this type of reaction, that is a capture reaction without a potential energy barrier, is characterized by a rapid decline with increasing collision energy (Levine and Bernstein 1987). The resultant thermal rate constant often exhibits a negative temperature dependence. It is also worthwhile pointing out a few limiting cases that for (i) $\sigma_0(E_c)$ = constant (i.e. the hard-sphere model), (ii) $\sigma_0(E_c) \propto 1/E_c$, (iii) $\sigma_0(E_c) \propto (E_c)^{1/2}$ and (iv) $\sigma_0(E_c) \propto (E_c)^{-1/2}$ (i.e. the Langevin model for singly charged ion–molecule reactions), the temperature dependences of the corresponding thermal rate constants are (i) $k(T) \propto (T)^{1/2}$, (ii) $k(T) \propto (T)^{-1/2}$, (iii) $k(T) \propto T$ and (iv) $k(T)$ = constant respectively. A casual inspection of the measured excitation function can then give a quick clue about the kinetic behaviour for the reaction of interest.

2. Barrierless reactions

2.1. $CN + O_2 \rightarrow NCO + O$

The reaction of the cyano radical (CN) with O_2 is an important step in NO_x formation and destruction in fuel-rich flames, and in other combustion processes such as the burning of coal. It is also becoming one of the most thoroughly studied radical–radical four-atom reaction systems (Smith 1995). The reaction has three exothermic product channels:

$$CN + O_2 \rightarrow NCO + O, \quad \Delta H_0 = -13.7 \text{ kcal mol}^{-1}, \tag{7}$$

$$\rightarrow CO + NO, \quad \Delta H_0 = -110 \text{ kcal mol}^{-1}, \tag{8}$$

$$\rightarrow N + CO_2, \quad \Delta H_0 = -93 \text{ kcal mol}^{-1}. \tag{9}$$

It is generally believed that this reaction is dominated by channel (7) and that channel (9) is very unlikely.

In terms of the overall reaction rate, only quite recently has the kinetic behaviour of this reaction been accurately determined over a wide temperature range, from 13 to 4000 K (Sims and Smith 1988a, b, Atakan *et al.* 1989, Durant and Tully 1989, Davidson *et al.* 1991, Sims *et al.* 1992, 1994). It was found that the thermal rate constant is quite large and exhibits a non-Arrhenius negative temperature dependence, that is the rate constant decreases with increasing temperature. The exact origin of this negative temperature dependence is the subject of some controversy. By conventional wisdom, the large rate constant and negative temperature dependence suggest that the reaction proceeds through an intermediate complex on an attractive PES with no significant barrier to complex formation (Klippenstein and Kim 1993, Vallance *et al.* 1996). On the other hand, according to the rotationally adiabatic capture theory (Clary 1984, 1990, Stoecklin *et al.* 1991), a direct abstraction reaction could also exhibit a negative temperature dependence. In this theory, the state-specific rate coefficient decreases as the rotational state j of the reagent increases at a given temperature. As a result, the negative temperature dependence of the thermal rate constant arises from the Boltzmann averaging over the initial rotational state distribution, which shifts the population towards higher rotationally excited (i.e. less reactive) states with increasing temperature. Thus two opposite reaction mechanisms can rationalize the observed negative temperature dependence for this reaction equally well.

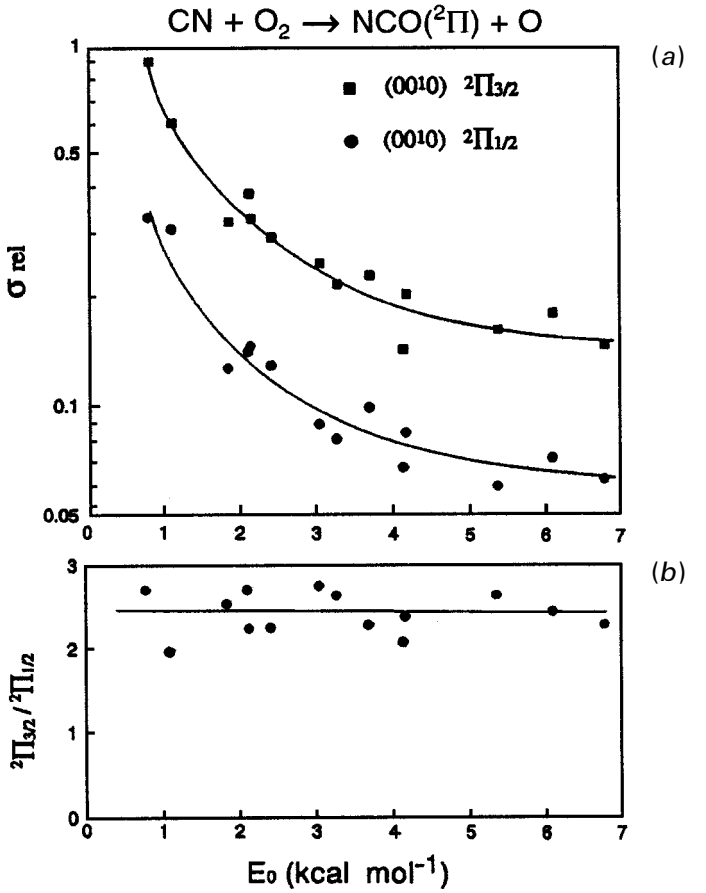

Figure 1. (*a*) Excitation functions for the ground vibronic state $^2\Pi_{3/2}$ (000) and the spin–orbit excited state $^2\Pi_{1/2}$ (000) of NCO from the CN+O_2 reaction. (*b*) Nearly identical energy dependences are seen for both vibronic product states.

Figure 1 shows the reactive excitation functions (Sonnenfroh and Liu 1991, Macdonald *et al*. 1994) for the formation of the vibronic ground and the spin–orbit excited states NCO $^2\Pi_{3/2}$ (000) and $^2\Pi_{1/2}$(000), which account for about 70% of the total yield for channel (1). Nearly identical energy dependences were also obtained for the other vibronically excited products (Macdonald *et al*. 1994). The (product) state-specific reaction cross-section is seen to decrease monotonically with the increase in collision energy over the energy range 0.7–7 kcal mol^{-1}. One immediate conclusion can be drawn that reaction (7) proceeds with little or no barrier. By fitting the excitation function with an analytic form and averaging it over Boltzmann translational energy distributions, the temperature dependence of a molecular-beam-derived thermal rate constant was deduced. The result and the available thermal rate constant data are compared in figure 2. What is remarkable about this comparison is the overall agreement between the beam-derived and the thermal rate constant data over such a wide temperature range. Even at the low- and high-temperature ends, the deviations are no more than 50%.

Because the beam-derived thermal rate constant refers to channel (7) only and the thermal kinetics data measure the overall reaction rate, the nearly perfect agreement

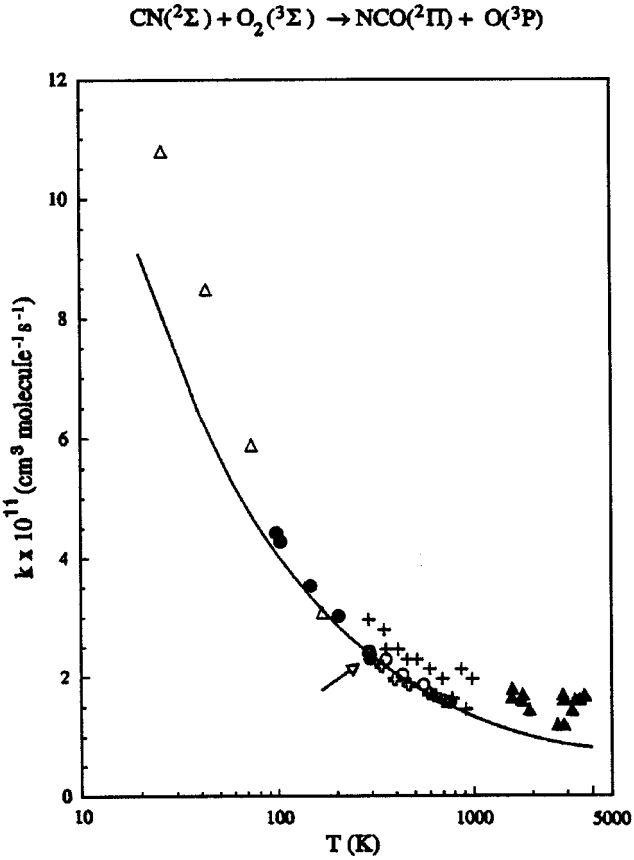

Figure 2. Comparisons of the beam-derived rate constant (——) with available thermal kinetics data (▲, △, ●, ○, +, ✙). The arrow indicates where the beam-derived result was normalized to the kinetic data. Note that the molecular beam result is for channel (7) only, and for essentially CN ($j = 0$) and O_2 ($j = 1$) reagents.

shown in figure 2 provides compelling evidence for the dominance of channel (7) in the reaction $CN+O_2$. In addition, figure 2 implies that the negative temperature dependence of this reaction is entirely determined by the translational energy dependence on the reaction cross-section for channel (7). It is instructive to elaborate this point a little. In the crossed-beam experiment (Macdonald *et al.* 1994) both the CN and the O_2 beams were from supersonic expansions; thus only the lowest few rotational states were present. Based on the discussion given above, since $k(T) \approx k_0(T)$, thus from equation (5) a near j independence of the rotational state-selected rate coefficient $k_j(T)$ is implied. This conclusion is in contrast with the prediction by the rotationally adiabatic capture theory (Stoecklin *et al.* 1991) but is in line with the expectation for a barrierless NCOO* complex-forming mechanism.

2.2. $Al(^2P)+O_2 \rightarrow AlO+O$

This reaction serves as an excellent illustration of the effect of spin–orbit reactivity for a barrierless reaction. The interest of this reaction lies in combustion chemistry, as Al is often used in liquid propellant slurries and in explosives. Several metal reactions involving Fe, Mg and Na recently also received considerable attention in

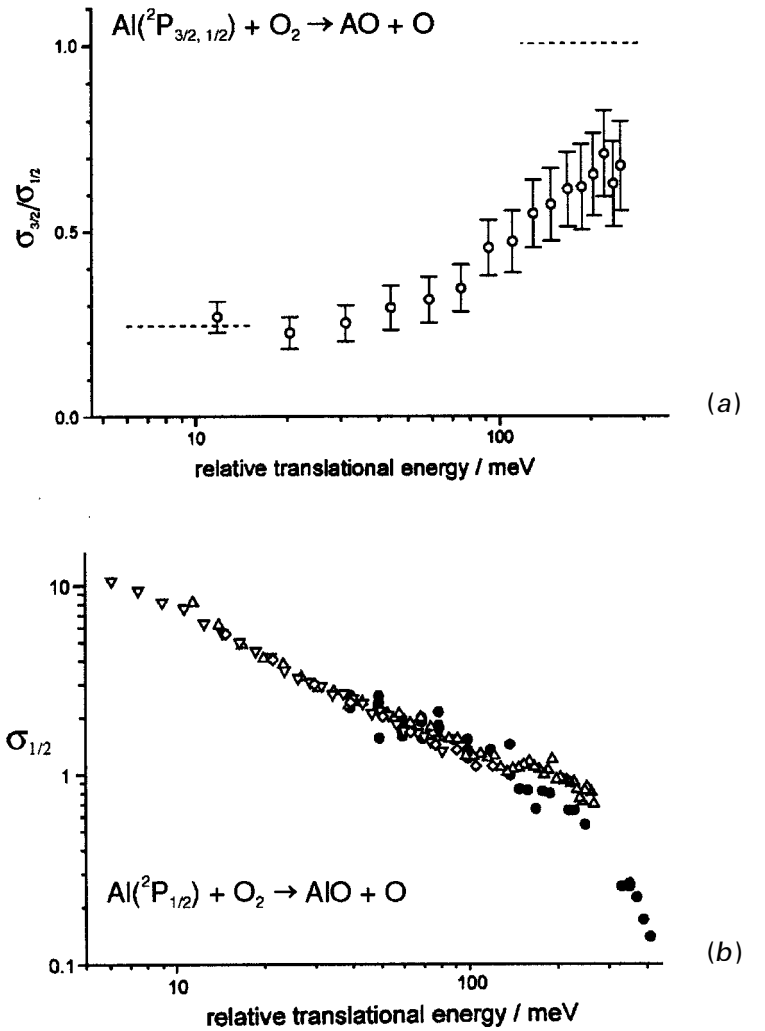

Figure 3. (*a*) The relative spin–orbit reactivity $\sigma_{3/2}/\sigma_{1/2}$ for the reaction $Al(^2P_{3/2}, ^2P_{1/2})+O_2 \rightarrow AlO+O$: (– – – –), adiabatic capture theory predictions in the high- and low-energy limits. (*b*) The excitation function for the ground spin–orbit reagent $Al(^2P_{1/2})$. (Adapted from Naulin and Costes (1999).)

interstellar chemistry (Plane 1991), because they are proposed to play a profound role in the evolution of metal-bearing molecules in interstellar dense clouds. Although the reaction of $Al+O_2$ is not among the list, its low-temperature kinetic behaviour could be regarded as a prototype for low-temperature metal chemistry.

The crossed-beam experiment was performed by the Bordeaux group (Naulin and Costes 1999). The Al beam was generated by the laser ablation technique. By using different carrier gases, Naulin and Costes were able to vary the spin–orbit contents $Al(^2P_{1/2})$ and $Al(^2P_{3/2})$, which lie about 0.014 eV above the ground state, in the beam, thus deducing their relative reactivities. Figure 3 shows the relative reaction cross-section $\sigma_{3/2}/\sigma_{1/2}$, and the excitation function for the ground spin–orbit Al ($^2P_{1/2}$) reagent. As is seen, the relative reactivity of the spin–orbit excited reagent remains finite at very low collision energies and increases gradually to a significant value with

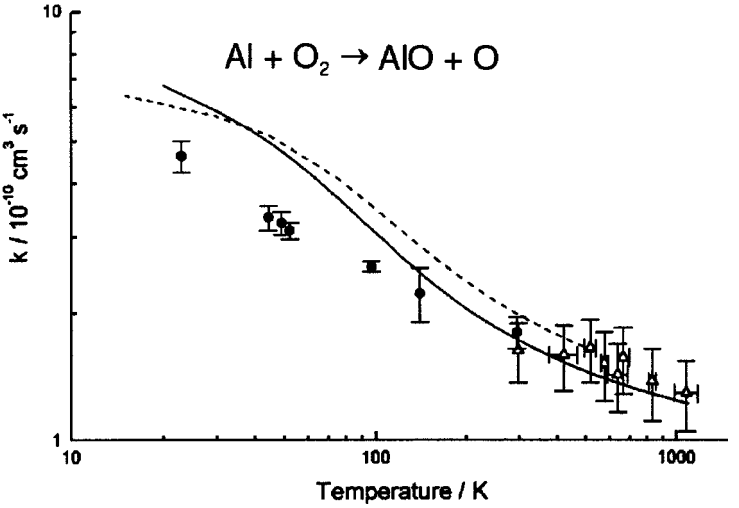

Figure 4. A comparison of the beam-derived rate constant (——) with thermal kinetics data (●, △) for the reaction $Al+O_2$: (– – – –), prediction from an adiabatic capture theory calculation. (Adapted from Naulin and Costes (1999).)

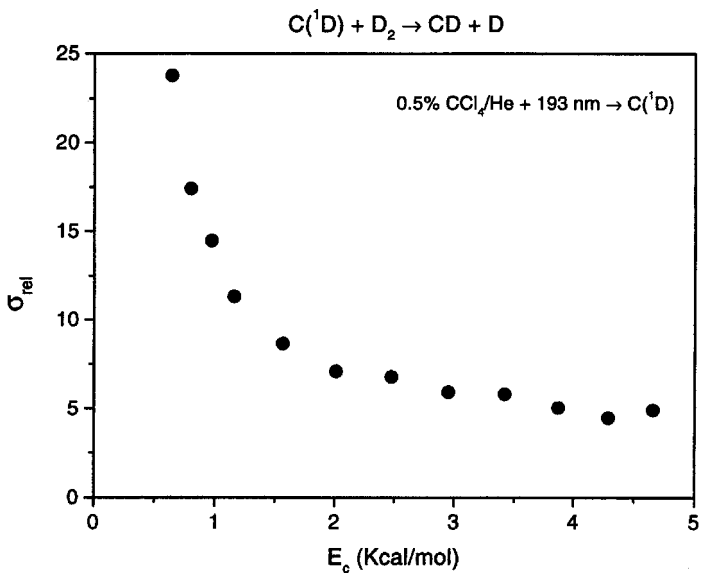

Figure 5. Excitation function for the $C(^1D)+D_2 \rightarrow CD+D$ reaction.

increasing energy. This finding is in contrast with an earlier report in which the spin–orbit excited $Al(^2P_{3/2})$ atom was concluded to be non-reactive towards O_2 molecules (Chen *et al.* 1995). Similar to the $CN+O_2$ reaction, the excitation function for $\sigma_{1/2}$ declines monotonically with increasing energy, and there is no sign of any activation energy to reaction even at a collision energy of 6 meV.

With a proper account for the thermal populations of the two spin–orbit states and their translational energy dependences of reaction cross-sections, a Boltzmann averaging was performed to obtain the beam-derived thermal rate constants. The results are shown in figure 4 together with the thermal kinetics data between 20 and

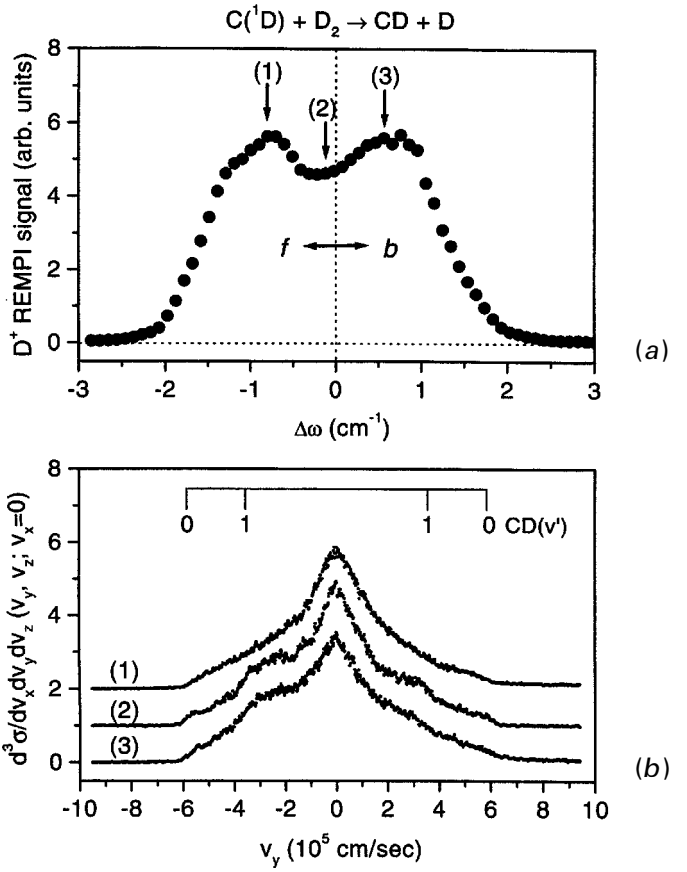

Figure 6. (*a*) The D-atom Doppler profile data taken under the '//configuration' for $C(^1D)+D_2$ at E_c = 4.5 kcal mol^{-1}: (----), partition of the forward and backward hemispheres of the product angular distribution. (*b*) Examples of a few Doppler-selected time-of-flight spectra of the D-atom product. The cap marked above indicates the energy limits of different vibration states of the co-product CD.

1100 K. Judging from the significant variation in the reactivities of the two spin–orbit states with collision energy, the excellent agreement shown in figure 4 signifies the important role of the spin–orbit excited state in the kinetics of this reaction. This conclusion is in accordance with theoretical investigations based on an approximate adiabatic capture theory (Le Picard *et al.* 1997, Reignier *et al.* 1998).

2.3. $C(^1D)+D_2 \rightarrow CD+D$

This reaction is slightly exoergic by $\Delta H_0 = -6.3$ kcal mol^{-1}. Electronically, the reagents and the products are correlated through an intermediate complex $CH_2(a\,^1A_1)$ lying about 100 kcal mol^{-1} below the reagent's asymptote. Thus, the reaction is expected to proceed through a side-on insertion mechanism involving a deep potential well, which is consistent with the general expectation for a divalent atom (Tsukiyama *et al.* 1985). A recent crossed-beam study of this reaction confirmed this expectation (Bergeat *et al.* 2000).

Figure 5 shows the excitation function for this reaction. The point to make here is to note the generation of the $C(^1D)$ beam. The primary photochemistry of CCl_4 at

193 nm is the production of CCl_3+Cl (Hintsa *et al.* 1991). Both radicals can potentially react with D_2, yielding the D-atom product. The reaction of CCl_3+D_2 is endothermic, thus requiring an internally hot CCl_3 radical to react (Xing *et al.* 1995), whereas the reaction of $Cl+D_2$ exhibits a sizeable activation barrier, as will be presented below. Neither reaction can readily account for the observation shown in figure 5. The proof that the observed signal arises indeed from the reaction $C(^1D)+D_2$ was from the differential cross-section measurements. Shown in figure 6(*a*) is the D-atom Doppler profile data taken under the '// configuration', that is the probe laser propagates along the direction of the relative velocity of the two reagents, at E_c = 4.5 kcal mol^{-1}. Its appearance suggests a forward–backward symmetric angular distribution, and its width is consistent with a maximal kinetic-energy release of 10 kcal mol^{-1}. Figure 6(*b*) displays a few examples of Doppler-selected time-of-flight spectra. As can be seen, distinct step features are readily identified. Energetically, they are entirely consistent with the formation of the different vibration states of $CD(v')$ from the $C(^1D)+D_2$ reaction at this collision energy. These observations, energetics and product angular distribution thus furnish the proof for the claimed reaction. Apparently, a mildly focused ArF laser (about 40 mJ or less) can easily strip off all four Cl atoms from CCl_4, yielding an excited $C(^1D)$ atom. It serves as a cautionary note in developing a 'clean' radical source for reaction studies (Liu *et al.* 1990).

From figures 5 and 6, one can conclude that the reaction of $C(^1D)+D_2$ proceeds as a barrierless insertion reaction. Although the temperature dependence of its rate is not available, judging from the shape of its excitation function, little temperature dependence is anticipated.

3. Activated reactions

3.1. $CN+D_2 \rightarrow DCN+D$

The reaction $CN+H_2 \rightarrow HCN+H$ ($\Delta H_0 = -21.6$ kcal mol^{-1}) and its isotopic variant have been studied extensively over the past few decades. The thermal rate constants exhibit a non-Arrhenius behaviour over the temperature range 250–3000 K (Sims and Smith 1988a, b, Sun *et al.* 1990, Szekely *et al.* 1983, Schadke *et al.* 1977, Wagner and Bair 1986). Theoretically, a recent PES, denoted as the TSH3 surface, was constructed for describing this reaction (ter Horst *et al.* 1996, Bethardy *et al.* 1997). The TSH3 surface is a PES empirically adjusted from high-quality *ab initio* calculations. It has a 3.2 kcal mol^{-1} barrier, and a quasiclassical trajectory (QCT) calculation based on the rate constants yielded, in excellent agreement with experimental kinetics data (ter Horst *et al.* 1996). On the other hand, good agreement with experimental results could also be obtained by a conventional transition-state rate calculation (He *et al.* 1998a, b) which is based on the *ab initio* barrier height of 4.2 kcal mol^{-1}. The observed curvature in the temperature dependence of the reaction rates was attributed to tunnelling effects and low-frequency bending modes at the saddle point. Thus, the actual barrier height for this reaction is a matter of debate.

Several other theoretical approaches, such as the time-dependent quantum wave-packet method (Light and Zhang 1998, Zhu *et al.* 1998a, b, Zhang and Lee 2000, Zhang *et al.* 2000a, b) and the flux correlation function method (Manthe and Matzkies 1998), were also performed for this reaction using the TSH3 surface. Based on the comparison with thermal kinetics data (good agreement at high temperatures, but significantly slower rates than experiments for lower temperatures), both studies concluded that the TSH3 PES is not quantitatively accurate in describing the reaction in the threshold region. Furthermore, using the flux correlation function method,

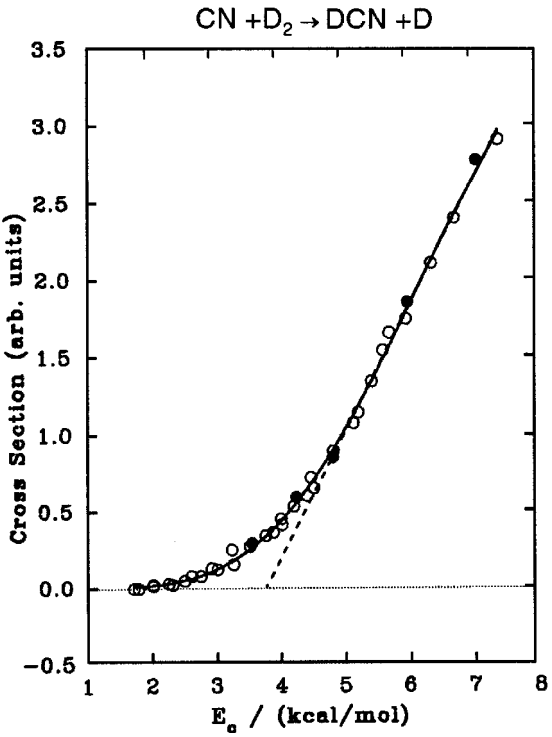

Figure 7. Excitation function for $CN+D_2 \rightarrow DCN+D$: (○), (●), data from two different types of measurement; (——), best fit; (– – – –), linear extrapolation with a threshold of around 4 kcal mol^{-1} by truncating the low-energy tail.

Manthe and Matzkies obtained bending frequencies of 150 and 460 cm^{-1}, which differ considerably from the frequencies 115 and 563 cm^{-1} from a normal mode analysis at the saddle point geometry of the TSH3 PES. These discrepancies signify problems in defining meaningful effective bending frequencies of the transition state in theoretical investigations of this reaction. Nevertheless, judging from the absence of any enhancement in the reaction rate by an increase in CN vibrational energies (Schadke *et al.* 1977, Sims and Smith 1988a, b) and the short reaction time from the wave-packet calculation, the reaction is ascribed as a direct abstraction with a collinear transition state located in the entrance channel with a barrier height of about 4 kcal mol^{-1} or less.

Dynamically, figure 7 depicts the excitation function for $CN+D_2 \rightarrow DCN+D$ (Che and Liu 1996). Its appearance is clearly consistent with an activation reaction, but a reaction barrier of about 2.5–3 kcal mol^{-1} appears to be significantly lower than the *ab initio* value of 4.2 kcal mol^{-1}. Ignoring the rotational state effects of the two reagents, the beam-derived rate constants can be obtained and compared with thermal kinetics data. The results are shown in figure 8. Two kinds of comparison are made to clarify the observed discrepancy. The solid curve represents the result from the full excitation function, while truncating the low-energy tail through a linearly extrapolated line, as indicated in figure 7, produces the dotted curve. It is interesting to note that the truncated excitation function is actually in good agreement with a subsequent full-dimensional quantum result for $CN+D_2$ reaction using the TSH3 PES (Zhu *et al.* 1998a, b). Both are arbitrarily normalized to room-temperature kinetic data for comparison. Apparently, the truncated curve exhibits an Arrhenius

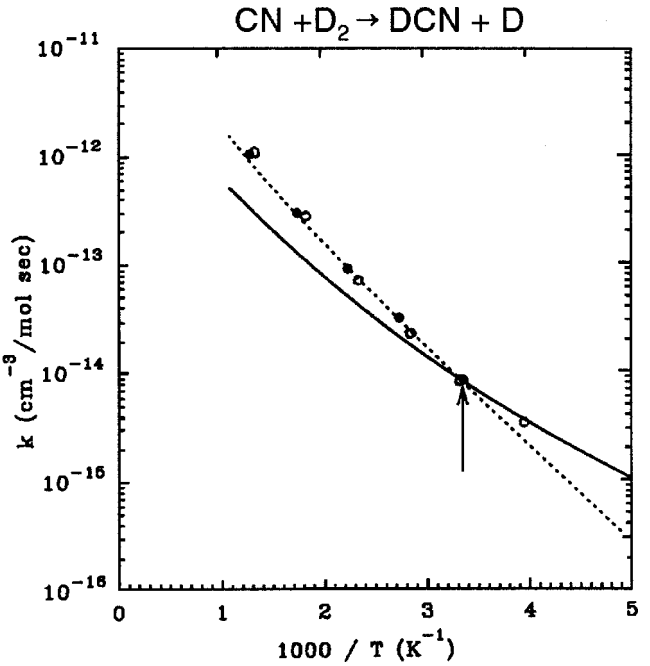

Figure 8. The comparison of the beam-derived rate constants with thermal kinetics data (○, ●): (——), line derived from the corresponding solid line in figure 7; (– – – –), line derived from the corresponding broken line in figure 7. The arrow marks the normalization point.

behaviour over this limited temperature range with a slope closely resembling that for the higher-temperature kinetics data. On the other hand, the result based on the full excitation function seems to display a slight curvature as suggested by kinetic studies and matches well for low-temperature kinetics data and yet deviates significantly at higher temperatures. It should be emphasized that the discrepancy between the dynamics measurement and thermal kinetics results is solely experimental. Thus, it is completely independent of the inaccuracy of the TSH3 PES and the theory–kinetics comparison as alluded to earlier. Based on these comparisons and the consideration of the anisotropy of interactions *en route* to the reaction barrier, it was conjectured (Che and Liu 1996) that the differences in the initial CN rotational state distributions and associated stereodynamics in the entrance valley could be one of the plausible origins for the apparent discrepancy between the beam-derived and thermal kinetics results. Although the subsequent theoretical investigations based on the TSH3 surface did not support this conjecture, the differential cross-section measurements appeared to confirm the vital role the CN rotation played in this reaction (Che and Liu 1995, 1996, Lai *et al.* 1996, Wang *et al.* 1997a, b).

3.2. $Cl(^2P)+H_2 \rightarrow HCl+H$

The title reaction is endothermic by 1.03 kcal mol^{-1} and has a rate of 1.6×10^{-14} cm^3 molecule^{-1} s^{-1} at 298 K. It is an important elementary step in the H_2–Cl_2 chain reaction. This reaction and its isotopic variations played a central role in the early development of transition-state theory and also served as a textbook example of the kinetic isotope effect (Johnston 1966). The thermal rate constants for the Cl+H_2 and D_2 reactions have recently been summarized over a wide temperature range from

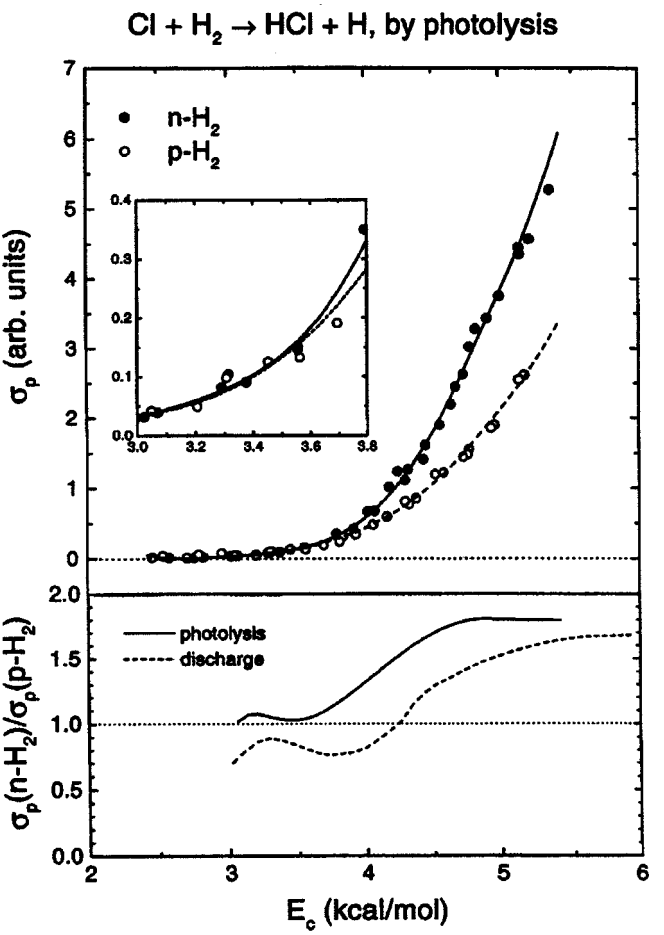

Figure 9. Excitation functions for the $Cl(^2P_{3/2})+n\text{-}H_2/para\text{-}H_2 \rightarrow HCl+H$ reactions.

200 to 3000 K (Kumaran *et al.* 1994). The temperature dependency is non-Arrhenius. Nevertheless, an activation energy of 4.4 kcal mol^{-1} can be deduced from the lower-temperature (below 500 K) results. Since then, this whole set of kinetics data has continued to provide a critical testing ground for formulating new theoretical methods in calculating thermal rate constants (Allison *et al.* 1996, Aoiz and Banares 1996, Lin *et al.* 1999, Manthe *et al.* 1999, Mielke *et al.* 1996, Wang *et al.* 1997a, b, Yang *et al.* 2000).

Figure 9 depicts the normalized excitation functions for the two different forms of H_2 (Lee *et al.* 1999). The Cl-atom beam was generated by photolysing Cl_2 at 355 nm; thus only the spin–orbit ground state $Cl(^2P_{3/2})$ is present. The normal H_2 consists of 75% of odd-j states (mostly $j = 1$) and 25% of even-j states (mostly $j = 0$) owing to nuclear spin statistics. The para-H_2 is mostly $j = 0$ with a small fraction of $j = 2$. The fact that the reaction of $Cl(^2P_{3/2})$ with n-H_2 exhibits a larger cross-section than that with para-H_2 implies a beneficial role of the H_2 rotation in promoting the reaction. This conclusion is in sharp contrast with the theoretical prediction (Aoiz and Banares 1996) of a negative influence of the reagent's rotation on reactivity based on a semiempirical G3 PES (Allison *et al.* 1996) but is in line with that based on a more recent fully *ab initio* BW2 PES (Bian and Werner 2000).

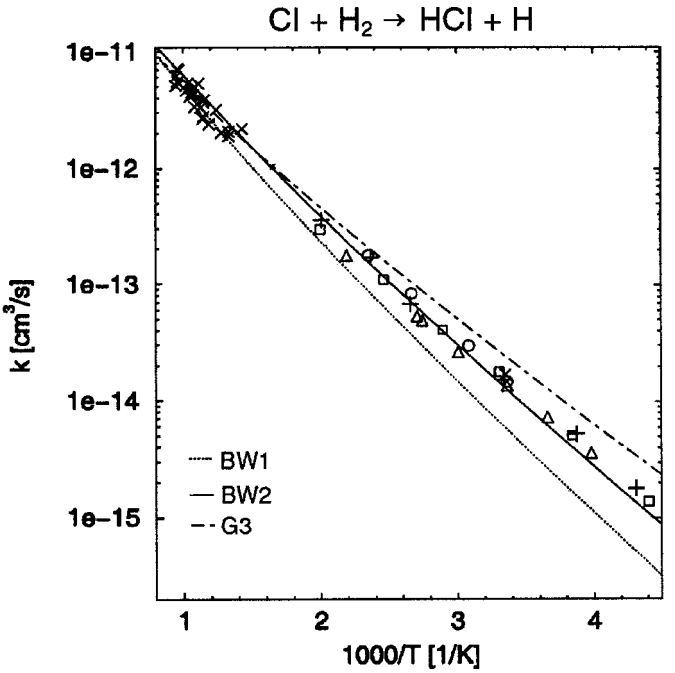

Figure 10. The comparison of the thermal rate constant for the reaction $Cl+H_2$: (×), (□), (+), (△), (○) experimental data; (· · · · ·), QM calculations on BW1 surfaces; (——), QM calculations on BW2 surfaces; (–·–), QM calculations based on G3 surfaces. (Adapted from Manthe *et al.* (1999).)

The characteristics of these two PESs are quite similar. Both exhibit a collinear barrier in the transition-state region, with the classical barrier heights of 7.61 and 7.88 kcal mol^{-1} for BW2 and G3 PES respectively. In terms of the geometry and the vibration frequencies near the saddle points, both surfaces are also nearly identical, except that the G3 barrier is somewhat narrower. Because of the similarity of the barrier properties of the G3 and BW2 PESs, transition-state theory will then predict nearly identical thermal rate constants for the two surfaces. As shown in figure 10, this expectation is nicely borne out by accurate quantum-mechanical (QM) calculations. Although somewhat higher reactivities at lower temperatures for the G3 surface could be attributed to more tunnelling through a narrower barrier, the general agreements between the G3 and BW2 predictions and with kinetic experiments also reflect the insensitivity of thermal kinetics data to the fine details of the PES. In particular, it is insensitive to the anisotropy of the interaction in the entrance valley, *vide infra*.

As mentioned above, the two surfaces predict opposite j dependences in reactivity; the H_2 rotation has a positive (or negative) influence on reactivity for the BW2 (or G3) PES. Through detailed analysis of trajectories, these different behaviours can be traced to the anisotropy of interactions *en route* to reaction barriers of the two surfaces. The semiempirical G3 PES is of the London–Eyring–Polanyi–Sato (LEPS) type at long range and thus exhibits little anisotopic interaction in the entrance channel. On the other hand, a T-shaped van der Waals well with a depth of 0.51 kcal mol^{-1} is found on the *ab initio* BW2 PES. Hence, as the Cl atom approaches a non-rotating H_2 reagent, the trajectories on the BW2 PES tend to be deflected away from the collinear transition state, resulting in a smaller reaction probability than those on the G3 PES. Furthermore, the shape of the anisotropy of the long-range interaction

on the BW2 surface is such that the rotation of the H_2 reactant helps to steer the trajectory into the reactive cone of acceptance, thus enhancing the reactivity. On the other hand, dynamical investigations using the G3 PES predicted the opposite (Aoiz and Banares 1996). The crossed-beam results shown in figure 9 clearly indicate that the reaction of $Cl(^2P_{3/2})+H_2$ is better described by the BW2 PES. Hence, the good agreement of the G3 thermal rate constants with the BW2 results is in fact a fortuitous error cancellation in Boltzmann averaging over the rotationally state-specific rate coefficients. In other words, the G3 surface erroneously predicts too large a value of $k_0(T)$ and a decreasing trend of $k_j(T)$ for higher j values. This example illustrates how sensitive the state-specific excitation function could be in differentiating different PESs which yield seemingly identical thermal rate constant data.

3.3. *F+HD → HF+D and DF+H*

The reaction of $F+H_2 \rightarrow HF+H$ is one of the most studied chemical reactions in science (Levine and Bernstein 1987), and the interest in this reaction dates back to the discovery of chemical laser. The kinetics of this reaction have been investigated extensively over past decades. A recent review (Persky and Kornweitz 1997) critically evaluated literature data, recommending for the temperature range 190–376 K the expression $k(T) = 1.1\times10^{-10}\exp(-450/T)$ cm^3 molecule^{-1} s^{-1} for the reaction $F+H_2$, and $k(T) = 1.06\times10^{-10}\exp(-635/T)$ cm^3 molecule^{-1} s^{-1} for $F+D_2$. Although no experimental determination of the thermal rate constant for F+HD is available, the intramolecular kinetic isotope effect was reported (Persky 1973). It was recommended that $k_{HF+D}/k_{DF+H} = 1.26\exp(35/T)$, which is nearly independent of temperature over the range 159–413 K.

Figure 11 presents the excitation functions for both isotope channels of the title reaction (Dong *et al.* 2000, Skodje *et al.* 2000a, b), together with theoretical predictions. Both QCT and QM calculations were based on the currently most accurate SW PES (Stark and Werner 1996). Quite apparent in the HF+D product channel is a distinct step near $E_c \approx 20$ meV. This feature is entirely absent in the QCT simulation and hence is suggestive of a QM origin. Indeed, theoretical predictions indicate a reaction barrier lying at around 45 meV, which situates this step feature in the tunnelling energy regime. A much more gradual increase in experimental $\sigma(E_c)$ is observed for $E_c \gtrsim 45$ meV, which is consistent with the onset of direct over-the-barrier reaction. By way of contrast, there is no hint of any step-like feature for the DF+H product channel, and its general appearance is in accord with the QCT simulation. The quantum prediction for this channel is seen to reproduce the experiment perfectly. As to the HF+D channel, the step-like peak is also well reproduced in position and shape but is too large in relative magnitude by a factor of about two. The origin of this discrepancy is suspected to be due to too narrow a barrier width predicted by the SW PES, which yields excess tunnelling and, hence, too large a reaction cross-section. Through detailed analysis of the QM results, it was demonstrated (Skodje *et al.* 2000a) that the physical origin of the step-like feature arises from a long-sought resonance of this reaction in the transition-state region. This is the first clear experimental evidence of reactive resonance for any chemical reaction in a full collision experiment.

Because the step-like peak was shown to be entirely attributed to resonance and this feature occurs only for the HF+D product channel at very low collision energies, it is reasonable to expect that it must have noticeable effects in thermal kinetics at low temperatures. One measure of such effects is the temperature dependence of the

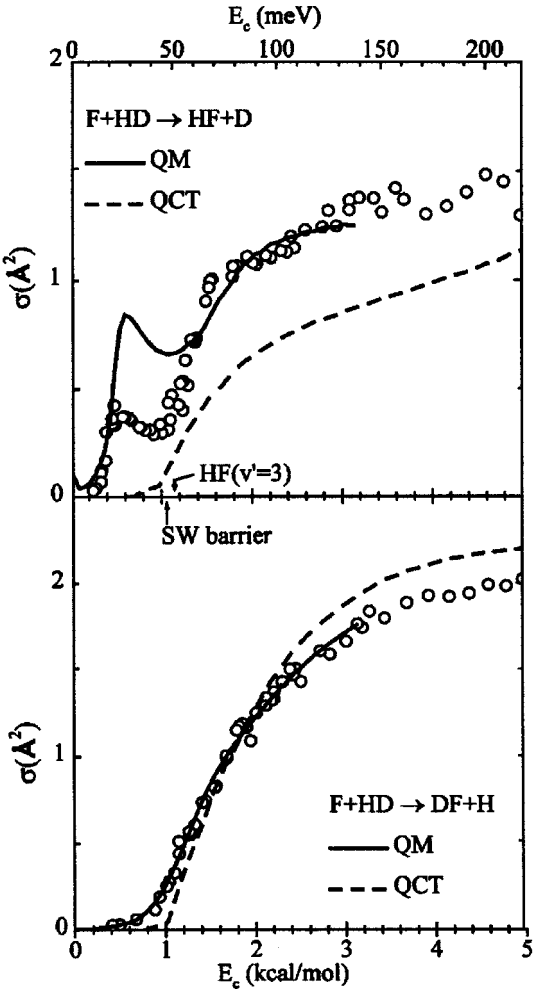

Figure 11. Excitation functions for the two isotopic channels of the F+HD reaction: (○), experimental results; (——), QM simulations on the SW PES; (– – –), QCT simulations on the SW PES.

intramolecular kinetic isotope effect, which is shown in figure 12. Both experiment and theory indicate that HF+D is the preferred product channel. At 400 K, the theoretical isotope ratio is also in good agreement with experiment. However, the theoretical ratio apparently rises too rapidly with the decrease in temperature. As a result, by 160 K the predicted isotope ratio becomes a factor of about two larger than the experiment. Based on a resonance model (Skodje *et al.* 2000a, b), it has been shown that the thermal rate constant at low temperature ($T < 200$ K) is almost entirely dominated by the contribution from resonance (R. T. Skodje, unpublished result). Because the QM excitation function overestimates the magnitude of the step-like feature (i.e. the resonance) by a factor of two (figure 11), the discrepancy in the kinetic isotope effect shown in figure 12 is then entirely consistent with the findings from dynamics studies. Future kinetics studies of this reaction at even lower temperatures ($T < 150$ K) will prove particularly rewarding. A more dramatic temperature variation in the intramolecular kinetic isotope effect than the current range should be observed.

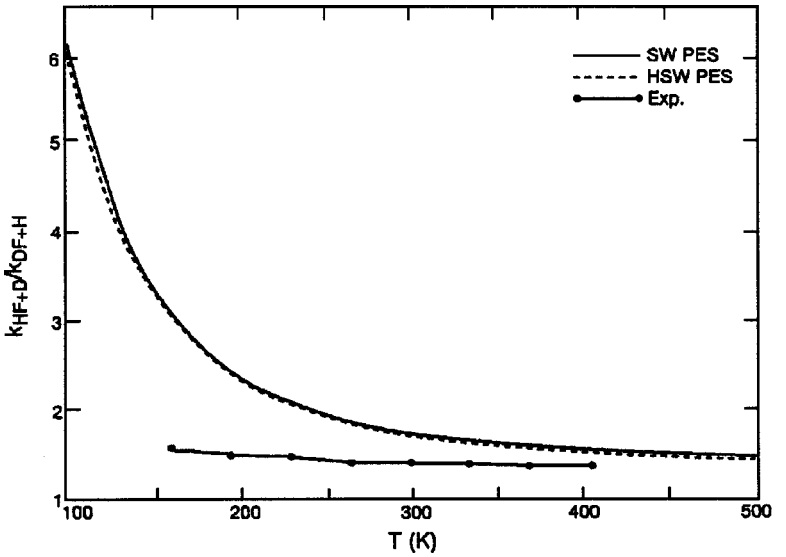

Figure 12. A comparison between QM and experimental results of intramolecular kinetic isotope effects k_{HF+D}/k_{DF+H} as a function of temperature. (Adapted from Zhang *et al.* (2000a).)

3.4. $N(^2D)+D_2 \rightarrow ND+D$

Gas-phase reactions of 'active nitrogen', particularly the lowest electronically excited $N(^2D)$ atom, with inorganic and organic molecules are of importance in a wide variety of applications such as the chemistry of interstellar clouds, the combustion of nitrogen-containing fuels and atmospheric chemistry. The simplest reaction, $N(^2D)+H_2 \rightarrow NH(X\,^3\Sigma^-)+H$, serves as a prototype and, as such, it has received much attention since the early 1970s. The kinetics data of this reaction were recently evaluated (Herron 1999), recommending $k(298\ K) = 2.2\times10^{-12}$ cm^3 molecule^{-1} s^{-1} with an activation energy of 2.5 kcal mol^{-1} for $N(^2D)+H_2$, and $k(298\ K) = 1.4\times10^{-12}$ cm^3 molecule^{-1} s^{-1} with 2.7 kcal mol^{-1} activation energy for $N(^2D)+D_2$. The question of abstraction versus insertion reaction mechanism has been the subject of controversy. More recently, both theory (Honvault and Launay 1999, Pederson *et al.* 1999, 2000) and dynamics experiments (Umemoto and Matsumoto 1996, Alagia *et al.* 1999) indicate that this reaction is in fact dominated by insertion. Electronically, the interaction of $N(^2D)$ with H_2 correlates with the $NH(^3\Sigma^-)+H$ through a deep well corresponding to the $NH_2(1\,^2A'')$ intermediate complex. Dynamically, a non-inverted product vibration distribution was measured (Umemoto and Matsumoto 1996), and a forward–backward symmetric angular distribution which is characteristic of a complex-forming reaction was also observed (Alagia *et al.* 1999). All these are consistent with an insertion mechanism, and yet thermal kinetics data also indicate a moderate activation energy. Hence, unlike several other more familiar barrierless insertion reactions, such as $C(^1D)+H_2$ (section 2.3), $S(^1D)+H_2$ and $O(^1D)+H_2$ (section 4), the present reaction $N(^2D)+H_2$ appears to be an activated insertion reaction.

Figure 13 presents the excitation function for $N(^2D)+D_2$. The radical beam was generated by 193 nm photolysis of a mixture of gases containing HNO_3. Our initial intention was to study the reaction of $OH+D_2$. This is a standard method for

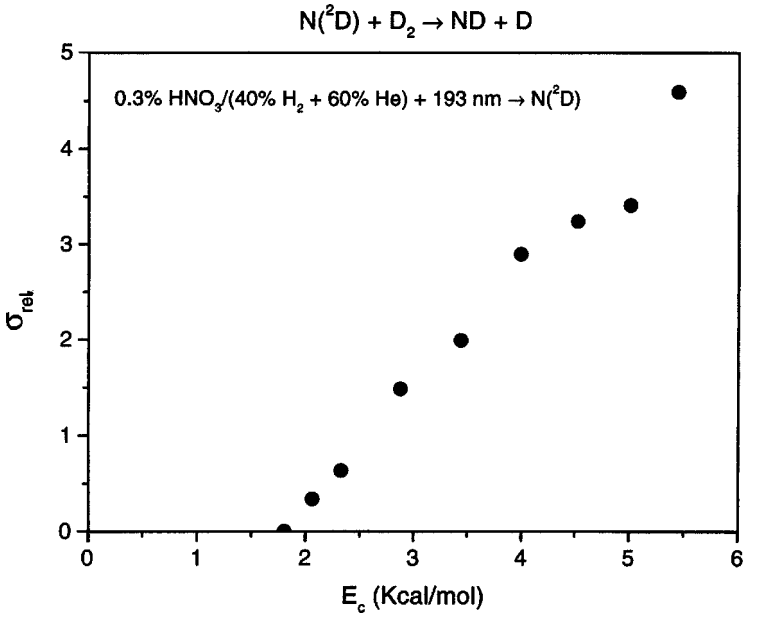

Figure 13. Excitation function for the reaction $N(^2D)+D_2 \rightarrow ND\ (X\ ^3\Sigma^-)+D$. The reaction $OH+D_2$ could also contribute to the observed D-atom product signals for $E_c >$ 4 kcal mol^{-1}.

generating an OH beam by photolysing the HNO_3 precursor molecule (Liu *et al.* 1990, Whitehead 1996). It is known that the excited $O(^1D)$ atom can also be formed. Thus, some H_2 molecules were added to the gas mixture to convert $O(^1D)$ into OH through the $O(^1D)+H_2$ reaction during the supersonic expansion. Although the measured excitation function indicated that an activated reaction is responsible for the observed signal, the threshold (4 kcal mol^{-1} or higher) appears too low for the targeted reaction $OH+D_2$. Differential cross-section measurements at E_c = 4.2 kcal mol^{-1} were then performed. These are not shown but are similar to those presented in figure 6. Both the product angular distribution (a forward–backward symmetric distribution) and the translational energy distribution are consistent with the reaction $N(^2D)+D_2 \rightarrow ND+D$. Although one cannot rule out the possibility that the $OH+D_2$ reaction also makes contributions at higher collision energies, the measured excitation function, at least for $E_c \lesssim 4$ kcal mol^{-1}, must be dominated by the $N(^2D)+D_2$ reaction. If one accepts this interpretation, one is led to conclude that this reaction has a reaction barrier of 2 kcal mol^{-1}. This conclusion is consistent with the activation energy (2.7 kcal mol^{-1}) deduced from the thermal kinetics data and with a high level *ab initio* PES calculation, 2.3 kcal mol^{-1} (Pederson *et al.* 1999).

4. More complicated reactions

The last example deals with the $O(^1D)+H_2$ reaction. In addition to its great importance in practical disciplines, this reaction is one of the best-known complex-forming reactions from a fundamental point of view (Levine and Bernstein 1987). Consequently, over the past decades this reaction has been exhaustively studied both experimentally and theoretically. Until very recently, it was regarded as the benchmark for insertion reactions.

Figure 14 summarizes the normalized excitation functions for the reactions

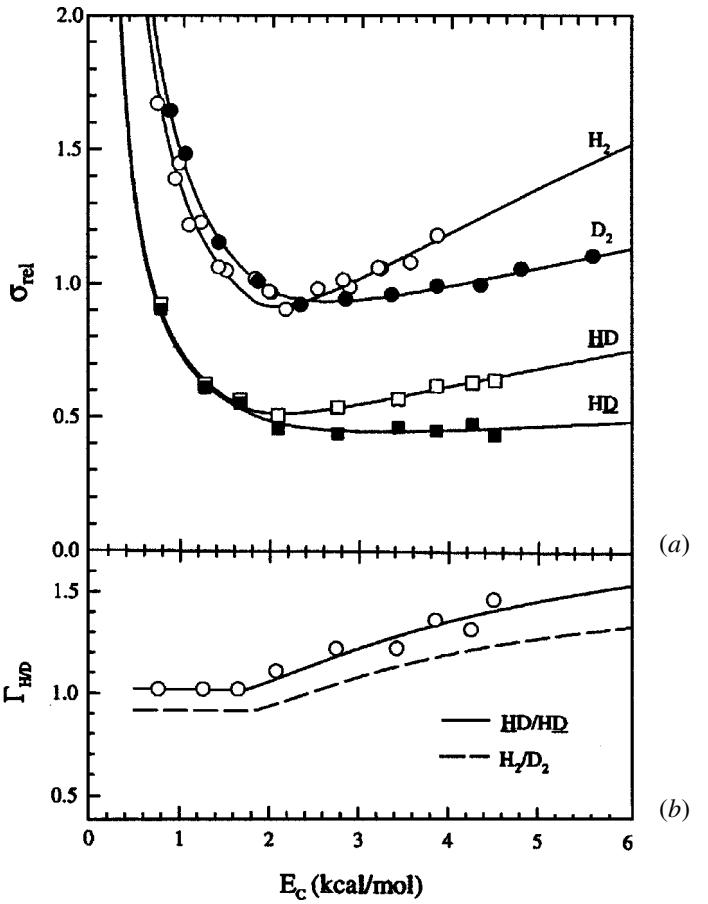

Figure 14. (*a*) Excitation functions and the ratio of H-to-D yields for the reactions $O(^1D)+H_2$, D_2 and HD. The label H D (H D) indicates when the H atom (D atom) is the leaving atom. (*b*) The isotope branching ratio $\Gamma_{H/D} = \sigma_H/\sigma_D$.

$O(^1D)+H_2/D_2 \rightarrow OH/OD+H/D$ and $O(^1D)+HD \rightarrow OH/OD+D/H$ (Hsu *et al.* 1997). The collision energy E_c here refers to the sum of the translational energy of the reagents and the small rotational energy of the target molecule. It implicitly assumes that the reagent rotational energy is as effective as the translational energy in promoting the reaction (Lee and Liu 1999). The excitation functions all display a peculiar energy dependence; the cross-section decreases rapidly at low energies, reaching a minimum near 2 kcal mol^{-1} and gradually increases afterwards, indicative of the interplay of two distinct reaction pathways. The hint of two pathways is also manifested in the isotope effect shown in figure 14 (*b*).

As exemplified in section 2, the rapid decrease in σ at low energies was interpreted as the characteristics of a capture reaction without a potential energy barrier. To account for the gradual increase in σ at higher energies, an additional direct abstraction pathway with a barrier of about 1.8 kcal mol^{-1} was postulated (Hsu *et al.* 1997). It was further conjectured that the abstraction corresponds to a reaction pathway occurring on the first excited singlet surface (1 Π) of this system. Two recent *ab initio* PESs, denoted K PES (Ho *et al.* 1996, Schatz *et al.* 1997) and DK PES (Dobbyn and Knowles 1997), appear to confirm this, both exhibit a collinear barrier of 2.3 kcal mol^{-1} on the

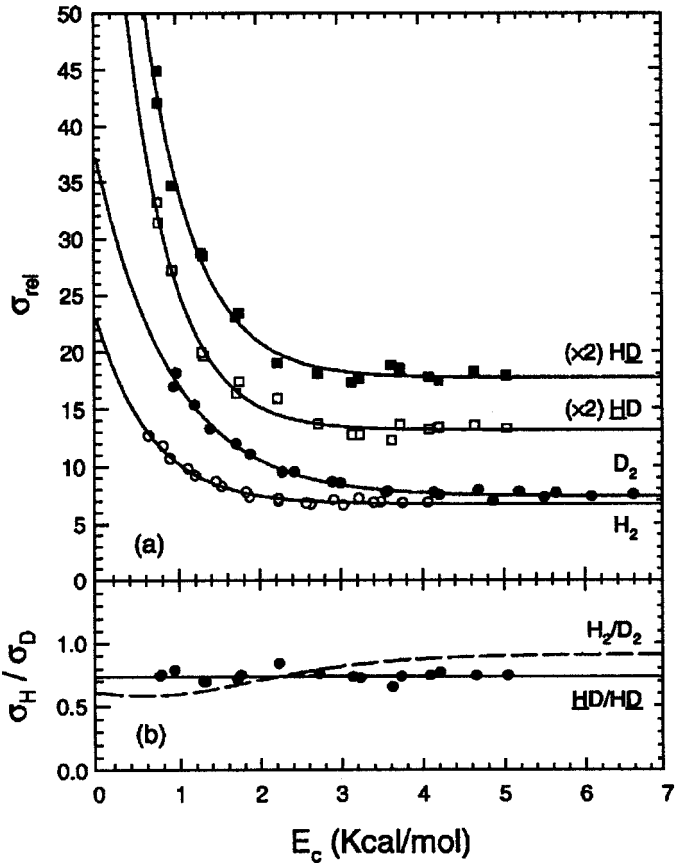

Figure 15. For the reactions $S(^1D)+H_2$, D_2 and HD. The labels are the same as in figure 14.

$1^1\Pi$ surface. Hence, the reaction of $O(^1D)+H_2$ at low energies is dominated by insertion but, at higher energies, a collinear abstraction pathway also makes significant contributions.

In this regard, it is instructive to compare the result of the $O(^1D)$ reaction with that of an analogous reaction of $S(^1D)$ (figure 15). In contrast with figure 14, the excitation functions for the $S(^1D)$ reaction behave in quite a 'normal' way, and the kinetic isotope effect displays little dependence on the collision energy (Lee and Liu 1998b, 2000). Apparently, the direct abstraction pathway is nearly absent for the $S(^1D)$ reactions over the energy range of this study. On intuitive grounds, the different reaction behaviours between $O(^1D)+H_2$ and $S(^1D)+H_2$ are not too surprising. The former is very exoergic, about 43 kcal mol^{-1}, whereas the latter is only so by 6.2 kcal mol^{-1}. If the abstraction pathway indeed occurs on a different surface from the insertive ground PES, in zeroth-order approximation these two pathways can be treated as being independent by neglecting the non-adiabatic coupling between them. According to the Evans–Polanyi (1938) relationship or the Hammond (1963) postulate one then expects that the activation energy on the $1^1\Pi$ surface should increase with decreasing exoergicity. Hence the collinear abstraction barrier for $S(^1D)+H_2$ should be much higher than that for $O(^1D)+H_2$. Indeed, a high-level *ab initio* calculation has recently been performed for the $S(^1D)+H_2$ reaction (Zyubin *et al.* 2001). The collinear barrier on the first excited $^1\Pi$ surface was found to be about 8 kcal mol^{-1}.

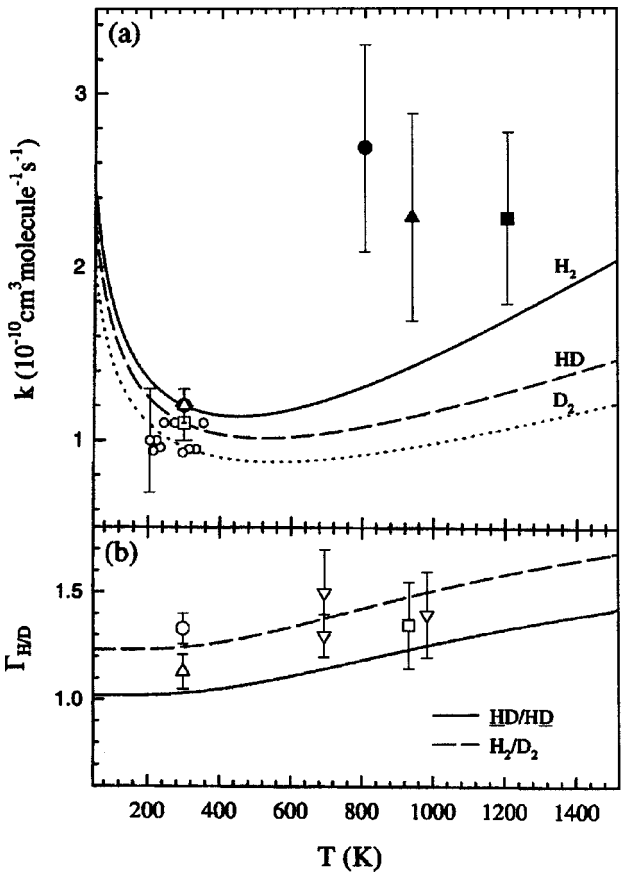

Figure 16. The corresponding comparison of the beam-derived results with thermal kinetics data for the $O(^1D)$ reactions.

Figure 16 compares the beam-derived thermal rate constants with the available kinetics data for the $O(^1D)$ reactions. At low temperatures, good agreement (i.e. within the quoted errors) was found in the kinetic isotope effect. Also apparent is the large body of kinetics data at higher temperatures (Koppe *et al.* 1993, Laurent *et al.* 1995) that were under dispute recently (Talukdar and Ravishankara 1996). Judging from the trend observed in the beam-derived rates, however, at least part of the discrepancies between the high-temperature and room-temperature kinetics measurements could be the manifestation of the contribution from the abstraction pathway.

5. Intramolecular kinetic isotope effects

Kinetic isotope effects have long been used to gain information on the shape of the PES for elementary chemical reactions (Johnston 1966, Johnston *et al.* 1991). It has also been recognized that, because of the large mass disparity of the H and the D atoms, the intramolecular isotope effect in the reaction A+HD provides a remarkably sensitive probe of the PES, sometimes much more so than the absolute rate constants or product state distributions. A few examples were given above. In this section we shall summarize the current status and take a closer look at this subject.

Table 2 summarizes the intramolecular isotope branching (AD+H)-to-(AH+D) ratio for a number of elementary chemical reactions of A+HD type. Both the crossed-

Table 2. Intramolecular isotope branching ratio for the A+HD reaction.

		(AD+H)-to-(AH+D) ratio		
A	Mechanism	Crossed-beam	Kinetics (298 K)	Reference
$C(^1D)$	Insertion		1.6	Sato *et al.* (1998)
$N(^2D)$	Insertion		1.5	Umemoto (1998)
$S(^1D)$	Insertion	0.72[a]	0.9–1.0	Lee and Liu (1998b, 2000); Inagaki *et al.* (1994)
$O(^1D)$	Insertion	1.17[a]	1.13–1.33	Hsu *et al.* (1997); Talukdar and Ravishankara (1996); Tsukiyama *et al.* (1985)
	Abstraction	≈ 2.8[b]		Hsu *et al.* (1997)
$F(^2P)$	Abstraction	$\lesssim 1.4$[b]	0.8	Skodje *et al.* (2000a); Persky and Kornweitz (1997)
$Cl(^2P)$	Abstraction	≈ 3[b]	0.6	Skouteris *et al.* (1999); Stern *et al.* (1973); Taatjes (1999)
$OH(^2\Pi)$	Abstraction	1.2[c]	0.35	Talukdar *et al.* (1996); Brownsword *et al.* (1997)
$CN(^2\Sigma)$	Abstraction		0.56	He *et al.* (1998a,b)

[a] Independent of collision energy.
[b] A strong function of collision energy and, thus, an averaged ratio is given here.
[c] Hot-atom experiment at $E_c = 0.24$ eV.

beam and the thermal kinetics results are listed. Despite the fact that this is a rather small set of data, several interesting trends are already apparent. First, in terms of thermal kinetics, the AD+H isotope channel is always the (slightly) preferred product for insertion, and the reverse is true for a direct abstraction reaction. This is the rule first pointed out by Tsukiyama *et al.* (1985). Qualitative arguments, based on either the screening of the D atom by the H atom in a rotating HD molecule for an activated abstraction reaction or the escape probability from a HAD complex for a barrierless insertion reaction, were proposed to rationalize the observation. Particularly notable here is the reaction of $N(^2D)+HD$. As discussed in section 3.4, this reaction is an activated insertion reaction. The consistency of its isotope branching ratio with the other barrierless insertion reactions (i.e. those 'larger than one') seems to suggest that complex decomposition (rather than the barrier stereodynamics) is the dominating factor, which is in line with the arguments of Tsukiyama *et al.*

Second, under crossed-beam conditions, the propensity rule for isotope branching ratio appears to be reversed from thermal kinetics! Although the crossed-beam (AD+H)-to-(AH+D) ratios for insertion reactions still cluster around one, they tend to be on the lower side. The ratios for abstraction, on the other hand, are significantly larger than one. Furthermore, while the ratios for insertion display little dependence on collision energies, those for abstraction in general exhibit dramatic energy variations.

The apparent discrepancy between the thermal kinetics and the crossed-beam observations was attributed to the rotationally cold HD reagent in the latter experiment (Lee and Liu 1998b, 2000). The rotational temperature of our HD beam was estimated to be about 50 K, namely about 82% of $j = 0$ and 18% in $j = 1$. This is to be contrasted to the room-temperature Boltzmann distribution: only 20% in $j = 0$, or 80% for $j > 0$. In a very illuminating review, Levine (1990) discussed in great detail, for a collinear abstraction reaction, how the intramolecular isotope branching ratio depends on the shape of the PES *en route* to the barrier (i.e. oblate versus prolate), and the effect of the HD rotation on the isotope ratio. The mass asymmetry effects, which yield a larger cone of acceptance for attacking the D end, clearly play a dominant role in favour of the AD formation for $j = 0$ at low energies. The variation in the isotope ratio with collision energy arises from the reorientation effect, that is the stereodynamics exerted by the anisotropy of the long-range interaction in the entrance channel, which is more pronounced for attacking the H end because of the mass asymmetry. For a rotating reagent, the rotation of the HD molecule could enhance the overall reactivity, making the probabilities of attacking either end more nearly the same. The H-atom screening effect could also come into play. Both effects tend to lead to the opposite propensity for a rotating than for a non-rotating HD reagent, which is in accord with the experimental findings summarized in table 2. Clearly, in addition to the anisotropy of interaction *en route* to reaction barrier, the relative magnitudes of the rotational energy and the translational energy also play a vital role in governing the isotope branching ratio for a direct abstraction reaction (Aoiz *et al.* 1998). Hence, the very same steric effect should also manifest itself for the homonuclear reagents, H_2 and D_2. As presented in section 3.3, indeed a strong dependence of reactivity on the initial j state was found for the $Cl+H_2(j)$ reaction.

As to the complex-forming reaction, the lifetime of the intermediate complex needs to be considered. If it is long, all initial memory besides the total energy, total angular momentum and total parity will be lost. The steric imprint associated with the reaction barrier in the entrance valley will be diminished and, thus, little dependence of the

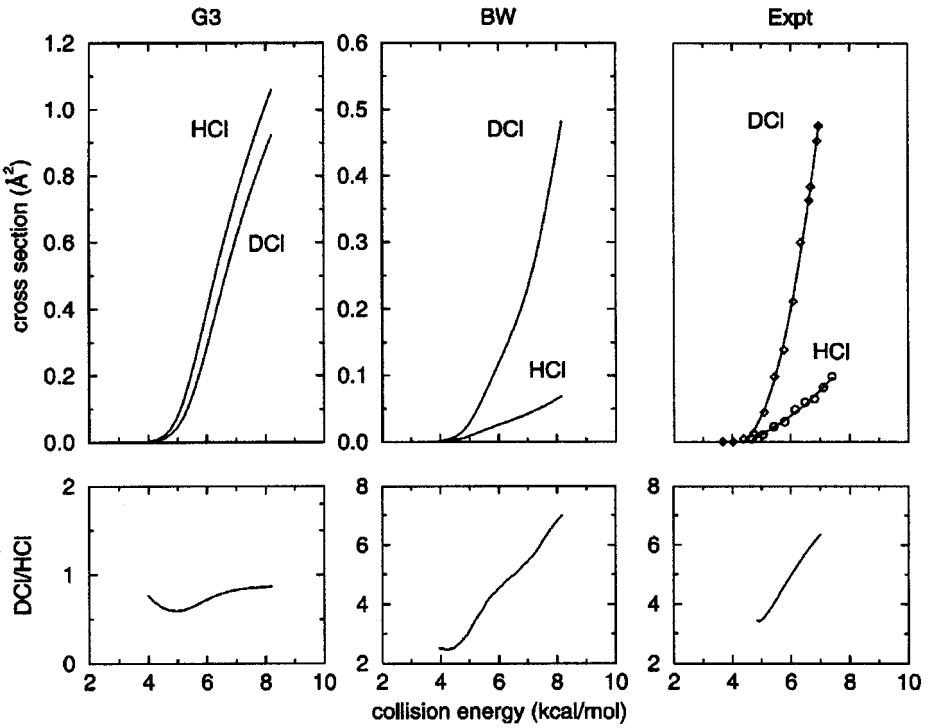

Figure 17. Comparison of theoretical and experimental excitation functions and the DCl-to-HCl product branching ratios for the Cl+HD ($v = 0$; 82% $j = 0$+18% $j = 1$) reaction.

intramolecular isotope branching on the initial rotational state or on the collision energy is anticipated. The same might hold for a barrierless reaction, regardless of its reaction mechanism or the lifetime of its intermediate complex (Lee and Liu 1998a). The complex decomposition would then play a more important role in governing the intramolecular isotope branching ratio. On the other hand, for an indirect reaction involved a short-lived complex and with an activation energy in the entrance channel, similar behaviours to an activated direct abstraction reaction could prevail. At least, the barrier stereodynamics could be in competition with the complex decomposition factors for intramolecular isotope effects. In this regard, it will be very rewarding to carry out further crossed-beam experiments to complete the comparison listed in table 2.

Before closing, we wish to reiterate that the intramolecular isotope branching and rotational state effect are just 'two sides of a coin'. Both are intimately related to stereodynamics exerted by the anisotropy of the long-range interaction in the entrance channel. Yet, one still wonders how large the anisotropy of the interactions should be. This is best exemplified by a recent report of the Cl+HD reaction (Skouteris *et al.* 1999). The crossed-beam experiment indicated a strong preference for the formation of DCl+H over HCl+D. Exact QM calculations on the two PESs yielded vastly different predictions (figure 17). While the result using the BW PES is in excellent agreement with experiment, the result on the G3 PES gives a nearly identical branching for the two isotope channels. As alluded to in section 3.3, the barrier properties of the two surfaces are essentially identical and their major differences lie in the van der Waals interaction region. Detailed dynamical analysis revealed that the

origin of the discrepancy of these two theoretical predictions could be entirely traced to the anisotropy of interactions in the entrance valley. Because the classical barrier height is about 7.7 kcal mol^{-1}, the van der Waals minimum of 0.5 kcal mol^{-1} in the entrance valley of the BW PES is less than 7% of the barrier height. It is truly remarkable that this comparatively small interaction can yield such a tremendous impact on scattering outcomes! The result shown in figure 17 serves as a proof-of-principle example for such a subtle and yet significant steric effect in a chemical reaction.

6. Concluding remarks

The reactive excitation function is highly averaged dynamical attribute which lies underneath the expression for the thermal kinetic rate constant. In this review, however, we have shown that invaluable insights can be gained through a proper comparison of these two quantities. This comparison could be particularly enlightening for the cases in which state-specific excitation functions are measured. A few rotation-specific examples were given in this review. It was argued that the stereoselectivity associated with the initial rotational state also manifests itself in the intramolecular isotope branching ratio of the isotopically analogous reaction. Since thermal kinetics measurements are available in general for more reaction systems than full dynamics studies, the simple comparison illustrated here should be readily applicable to many future excitation function measurements for gaining further information about intermolecular interactions.

A few general conclusions can be drawn from the limited number of systems that have been investigated. For an activated direct reaction, because of the nature of the saddle point, the anisotropy in the transition-state region and in the entrance valley could have profound stereodynamical effects on reactive behaviours. A strong dependence of reactivity on the initial rotational state is then anticipated. In this case, while the direct link between the excitation function (usually for cold reagents) and thermal kinetics could be problematic, a judicious comparison of these two sets of data can often provide invaluable information on the anisotropy of PES. Further measurements of the rotational state-specific excitation function and the intramolecular kinetic isotope branching ratio would be particularly fruitful. On the other hand, for a barrierless reaction, the interaction in the entrance valley is generally less anistropic. Hence, the dependence of reactivity on the initial rotational state becomes less. In this case, a simple Boltzmann averaging of the excitation function data from a crossed-beam experiment often leads to a reliable extrapolation of the thermal rate constant over the unavailable temperature range. Furthermore, the intramolecular isotope branching ratio for the A+HD type of reaction is around unity for both the crossed-beam and the kinetics measurements. Little variation in this ratio with the changes in collision energy and temperature appears to be the rule.

Acknowledgements

The National Science Council of Taiwan, Chinese Petroleum Corporation and the US Department of Energy, Office of Basic Energy Sciences, supported this work. The contributions of L.-H. Lai and S.-H. Lee to the preliminary results on $C(^1D)+D_2$ and $N(^2D)+D_2$ discussed herein are gratefully acknowledged. We are indebted to R. T. Skodje for communicating his unpublished result on the kinetic aspects of the F+HD reaction.

References

ALAGIA, M., BALUCANI, L., CARTECHINI, L., CASAVECCHIA, P., VOLPI, G. G., PETERSON, L. A., SCHATZ, G. C., LENDVAY, G., HARDING, L. B., HOLLE BEEK, T., HO, T.-S., and RABITZ, H., 1999, *J. chem. Phys.*, **110**, 8857.

ALLISON, T. C., LYNCH, G. C., TRUHLAR, D. G., and GORDON, M. S., 1996, *J. phys. Chem.*, **100**, 13 575.

AOIZ, F. J. and BANARES, L., 1996, *J. phys. Chem.*, **100**, 18 108.

AOIZ, F. J., BANARES, L., and HERRERO, V. J., 1998, *J. chem. Soc., Faraday Trans.*, **94**, 2483.

ATAKAN, B., JACOBS, A., WAHL, M., WELLER, R., and WOLFRUM, J., 1989, *Chem. Phys. Lett.*, **154**, 449.

BALLA, R. J., and PASTERNAK, L., 1987, *J. phys. Chem.*, **91**, 73.

BERGEAT, A., CARTECHINI, L., BALUCANI, N., CAPOZZA, G., PHILLIPS, L. F., CASAVECCHIA, P., VOLPI, G. G., BONNET, L., and RAYEZ, J.-C., 2000, *Chem. Phys. Lett.*, **327**, 197.

BETHARDY, G. A., WAGNER, A. F., SCHATZ, G. C., and TER HORST, M. A., 1997, *J. chem. Phys.*, **106**, 6001.

BIAN, W., and WERNER, H.-J., 2000, *J. chem. Phys.*, **112**, 220.

BROWNSWORD, R. A., HILLENKAMP, M., SCHMIECHEN, P., VOLPP, H.-R., and WOLFRUM, J., 1997, *Chem. Phys. Lett.*, **275**, 325.

CHE, D.-C., and LIU, K., 1995, *Chem. Phys. Lett.*, **243**, 290; 1996, *Chem. Phys.*, **207**, 367.

CHEN, K., SUNG, C, CHANG, J., CHUNG, T., and LEE, K., 1995, *Chem. Phys. Lett.*, **240**, 17.

CLARY, D. C., 1984, *Molec. Phys.*, **53**, 3; 1990, *Comments at molec Phys.*, **24**, 145.

DAVIDSON, D. F., DEAN, A. J., DIROSA, M. D., and HANSON, R. K., 1991, *Int. J. chem. Kinetics*, **23**, 1035.

DOBBYN, A. J., and KNOWLES, P. J., 1997, *Molec. Phys.*, **91**, 1107.

DONG, F., LEE, S.-H., and LIU, K., 2000, *J. chem. Phys.*, **113**, 3633.

DURANT, J. L., JR, and TULLY, F. P., 1989, *Chem. Phys. Lett.*, **154**, 568.

EVANS, M. G., and POLANYI, M., 1938, *Trans. Faraday Soc.*, **34**, 11.

GEPPERT, W. D., REIGNIER, D., STOECKLIN, T., NAULIN, C., COSTES, M., CHASTAING, D., LE PICARD, S. D., SIMS, I. R., and SMITH, I. W. M., 2000, *Phys. Chem. chem. Phys.*, **2**, 2873.

GONZALEZ-URENA, A., 1987, *Adv. chem. Phys.*, **LXVI**, 213; 1992, *J. phys., Chem.*, **96**, 8212.

HAMMOND, G. S., 1963, *J. Am. chem. Soc.*, **85**, 2544.

HE, G., HARDING, L. B., and MACDONALD, R. G., 1998a, *J. phys. Chem.* A, **102**, 7563.

HE, G., TOKUE, I., and MACDONALD, R. G., 1998b, *J. phys. Chem.* A, **102**, 4585.

HERRON, J. T., 1999, *J. phys. Chem. Ref. Data*, **28**, 1453.

HINTSA, E. J., ZHAO, K., JACKSON, W. M., MILLER, W. B., WODTKE, A. M., and LEE, Y. T., 1991, *J. phys. Chem.*, **95**, 2799.

HO, T. S. HOLLEBEEK, T., RABITZ, H., HARDING, L. B., and SCHATZ, G. C., 1996, *J. chem. Phys.*, **105**, 10 472.

HONVAULT, P., and LAUNAY, J.-M., 1999, *J. chem. Phys.*, **111**, 6665.

HSU, Y.-T., WANG, J.-H., and LIU, K., 1997, *J. chem. Phys.*, **107**, 2351.

INAGAKI, Y., SHAMSUDDIN, S. M., MATSUMI, Y., and KAWASAKI, M., 1994, *Laser Chem.*, **14**, 235.

JOHNSTON, G. W., KORNWEITZ, H., SCHECHTER, I., PERSKY, A., KATZ, B., BERSOHN, R., and LEVINE, R. D., 1991, *J. chem. Phys.*, **94**, 2749.

JOHNSTON, H. S., 1966, *Gas Phase Reaction Rate Theory* (New York: Ronald Press), chapter 13.

KLIPPENSTEIN, S. J., and KIM, Y.-W., 1993, *J. chem. Phys.*, **99**, 5790.

KOPPE, S., LAURENT, T., NAIK, P. D., VOLPP, H.-R., WOLFRUM, J., ARUSIPARPAR, T., BAR, I., and ROSENWAKS, S., 1993, *Chem. Phys. Lett.*, **214**, 546.

KUMARAN, S. S., LIM, K. P., and MICHAEL, J. V., 1994, *J. chem. Phys.*, **101**, 9487.

LAI, L.-H., WANG, J.-H., CHE, D.-C., and LIU, K., 1996, *J. chem. Phys.*, **105**, 3332.

LAURENT, T., NAIK, P. D., VOLPP, H.-R., WOLFRUM, J., ARUSIPARPAR, T., BAR, I., and ROSENWAKS, S., 1995, *Chem. Phys. Lett.*, **236**, 343.

LEE, S.-H., LAI, L.-H., LIU, K., and CHANG, H., 1999, *J. chem. Phys.*, **110**, 8229.

LEE, S.-H., and LIU, K., 1998a, *J. phys. Chem.* A, **102**, 8637; 1998b, *Chem. Phys. Lett.*, **290**, 323; 2000, *Chem. Phys. Lett.*, **317**, 516.

LE PICARD, S. D., CANOSA, A., TRAVERS, D., CHASTAING, D., ROWE, B. R., and STOECKLIN, T., 1997, *J. Phys. Chem.* A, **101**, 9988.

LEVINE, R. D., 1990, *J. phys. Chem.*, **94**, 8872.

LEVINE, R. D., and BERNSTEIN, R. B., 1987, *Molecular Reaction Dynamics and Chemical Reactivity* (Oxford University Press).
LIGHT, J. C., and ZHANG, D. H., 1998, *Discuss Faraday Soc.*, **110**, 105.
LIN, S.-Y., PARK, S. C., and KIM, M. S., 1999, *J. chem. Phys.*, **111**, 3787.
LIU, K., MACDONALD, R. G., and WAGNER, A. F., 1990, *Int. Rev. phys. Chem.*, **9**, 187.
MACDONALD, R. G., LIU, K., SONNENFROH, D. M., and LIU, D.-J., 1994, *Can. J. Chem.*, **72**, 660.
MANTHE, U., BIAN, W., and WERNER, H.-J., 1999, *Chem. Phys. Lett.*, **313**, 647.
MANTHE, U., and MATZKIES, F., 1998, *Chem. Phys. Lett.*, **282**, 442.
MIELKE, S. L., ALLISON, T. C., and TRUHLAR, D. G., 1996, *J. phys. Chem.*, **100**, 13 588.
NAULIN, C., and COSTES, M., 1999, *Chem. Phys. Lett.*, **310**, 231.
PEDERSON, L. A., SCHATZ, G. C., HOLLEBEEK, T., HO, T.-S., RABITZ, H., and HARDING, L. B., 1999, *J. chem. Phys.*, **110**, 9091; 2000, *J. phys. Chem.* A, **104**, 2301.
PERSKY, A., 1973, *J. chem. Phys.*, **59**, 5578.
PERSKY, A., and KORNWEITZ, H., 1997, *Int. J. chem. Kinetics*, **29**, 67.
PLANE, J. M. C., 1991, *Int. Rev. phys. Chem.*, **10**, 55.
REIGNIER, D., STOECKLIN, T., LE PICARD, S. D., CANOSA, A., and ROWE, B. R., 1998, *J. chem. Soc., Faraday Trans.*, **94**, 1681.
SATO, K., ISHIDA, N., KURAKATA, T., IWASAKI, A., and TSUNASHIMA, S., 1998, *Chem. Phys.*, **237**, 195.
SCHADKE, H., WAGNER, H. G., and WOLFRUM, J., 1997, *Ber. Bunsenges. phys. Chem.*, **81**, 670.
SCHATZ, G. C., PAPAIOANNOU, A., PEDERSON, L. A., HARDING, L. B., HOLLEBEEK, T., HO, T. S., and RABITZ, H., 1997, *J. chem. Phys.*, **107**, 23 740.
SIMS, I. R., QUEFFELEC, J. L., DEFRANCE, A., REBRIO-ROWE, C., TRAERS, D., ROWE, B. R., and SMITH, I. W. M., 1992, *J. chem. Phys.*, **97**, 8798; 1994, *ibid.*, **100**, 4229.
SIMS, I. R., and SMITH, I. W. M., 1988a, *Chem. Phys. Lett.*, **149**, 565; 1988b, *J. chem. Soc., Faraday Trans.* II, **84**, 527.
SKODJE, R. T., SKOUTERIS, D., MANOLOPOULOS, D. E., LEE, S.-H., DONG, F., and LIU, K., 2000a, *J. chem. Phys.*, **112**, 4536; 2000b. *Phys. Rev. Lett.*, **85**, 1206.
SKOUTERIS, D., MANOLOPOULOS, D. E., BIAN, W., WERNER, H.-J., LAI, L.-H., and LIU, K., 1999, *Science*, **286**, 1713.
SMITH, I. W. M., 1995, *The Chemical Dynamics and Kinetics of Small Radicals*, Part I, edited by K. Liu and A. F. Wagner (Singapore: World Scientific), chapter 6.
SONNENFROH, D. M., and LIU, K., 1991, *Chem. Phys. Lett.*, **176**, 183.
STARK, K., and WERNER, H.-J., 1996, *J. chem. Phys.*, **104**, 6515.
STERN, M. J., PERSKY, A., and KLEIN, F. S., 1973, *J. chem. Phys.*, **58**, 5697.
STOECKLIN, T., DATEO, C. E., and CLARY, D. C., 1991, *J. chem. Soc., Faraday Trans.*, **87**, 1667.
SUN, Q., YANG, D. L., WANG, N. S., BOWMAN, J. M., and LIN, M. C., 1990, *J. chem. Phys.*, **93**, 4730.
SZEKELY, A., HANSEN, R. K., and BOWMAN, C. T., 1983, *Int. J. chem. Kinetics*, **15**, 915.
TAATJES, C. A., 1999, *Chem. Phys. Lett.*, **306**, 33.
TALUKDAR, R. K., GIERCZAK, T., GOLDFARB, L., RUDICH, Y., MADHAVA RAO, B. S., and RAVISHANKARA, A. R., 1996, *J. phys. Chem.* A, **100**, 3037.
TALUKDAR, R. K. AND RAVISHANKARA, A. R., 1996, *Chem. Phys. Lett.*, **253**, 177.
TER HORST, M. A., SCHATZ, G. C., and HARDING, L. B., 1996, *J. chem. Phys.*, **105**, 558.
TSUKIYAMA, K., KATZ, B., and BERSOHN, R., 1985, *J. Chem. Phys.*, **83**, 2889.
UMEMOTO, H., 1998, *Chem. Phys. Lett.*, **292**, 594.
UMEMOTO, H., and MATSUMOTO, K., 1996, *J. chem. Phys.*, **104**, 9640.
VALLANCE, C., MACLAGAN, R. G. A. R., and PHILLIPS, L. F., 1996, *Chem. Phys. Lett.*, **250**, 59.
VETTER, R., NAULIN, C., and COSTES, M., 2000, *Phys. Chem. chem. Phys.*, **2**, 643.
WAGNER, A. F., and BAIR, R. A., 1986, *Int. J. chem. Kinetics*, **18**, 473.
WANG, H., THOMPSON, W. H., and MILLER, W. H., 1997, *J. chem. Phys.*, **107**, 7194.
WANG, J.-H., LIU, K., SCHATZ, G. C., and TER HORST, M., 1997, *J. chem. Phys.*, **107**, 7869.
WHITEHEAD, J. C., 1996, *Rep. Prog. Phys.*, **59**, 1.
XING, G., HUANG, X., BERSOHN, R., TSUKIYAMA, K., and KATZ, B., 1995, *J. chem. Phys.*, **102**, 3169.
YANG, B.-H., GAO, H.-T., HAN, K.-L., and ZHANG, J. Z. H., 2000, *J. chem. Phys.*, **113**, 1434.
ZHANG, D. H., and LEE, S.-Y., 2000, *J. chem. Phys.*, **112**, 203.
ZHANG, D. H., LEE, S.-Y., and BAER, M., 2000a, *J. chem. Phys.*, **112**, 9802.

ZHANG, Y., TAN, Z. ZHANG, Q., and ZHANG, J. Z. H., 2000b, *Chem. Phys.*, **252**, 191.
ZHU, W., ZHANG, J. Z. H., and ZHANG, D. H., 1998a, *Chem. Phys. Lett.*, **292**, 46.
ZHU, W., ZHANG, J. Z. H., ZHANG, Y. C., ZHANG, Y. B., ZHAN, L. X., ZHANG, S. L., and ZHANG, D. H., 1998b, *J. chem. Phys.*, **108**, 3509.
ZYUBIN, A. S., MEBEL, A. M., CHAO, S. D., and SKODJE, R. T., 2001, *J. chem. Phys.*, **114**, 320.